Available online at www.sciencedirect.com
SCIENCE DIRECT®
Journal of Sound and Vibration 269 (2004) 421–430
JOURNAL OF SOUND AND VIBRATION
www.elsevier.com/locate/jsvi

Letter to the Editor

Numerical prediction of centrifugal compressor noise

Hyosung Sun*, Soogab Lee

Department of Mechanical and Aerospace Engineering, Seoul National University, Shinlim-dong, Kwanak-gu, Seoul 151-742, South Korea

Received 23 October 2002; accepted 24 March 2003

1. Introduction

Experimental and analytical studies have been conducted to understand the characteristics of centrifugal compressor noise and to examine the influence of design parameters on the noise level [1,2]. The results reveal that BPF noise in relation to the impeller rotation plays an important role, which is found in the aeroacoustic study of noise generation through blade–tongue interaction and the effects of modifying the tongue and impeller geometries [3,4].

It is widely known that BPF noise components come from the circumferential flow distortions upstream and downstream of the impeller [5]. Present study focuses on the numerical investigation of this discrete noise. BEM solver coupled with Euler equations is introduced. The indirect variational BEM in the frequency domain is used to predict the inner and the outer noise propagation of the centrifugal compressor impeller.

The method of flow analysis will be discussed in the next section, followed by discussions on boundary element method (BEM), calculation results, and conclusions.

2. Flow solver

The unsteady, compressible, and three-dimensional Euler equations including impeller moving grid and patched grid are solved to analyze the flow unsteadiness due to circumferential inlet and outlet pressure distortions of the centrifugal compressor impeller. The system of equations consists of a local time derivative term and three convective flux vectors. In physical co-ordinates, the governing equation is

$$\frac{\partial Q}{\partial t}+\frac{\partial E}{\partial x}+\frac{\partial F}{\partial y}+\frac{\partial G}{\partial z}=0. \tag{1}$$

*Corresponding author. Tel.: +82-2-880-7384; fax: +82-2-875-4360.
E-mail address: aerosun@snu.ac.kr (H. Sun).

0022-460X/03/$ - see front matter
doi:10.1016/S0022-460X(03)00330-4

The convective terms are discretized using Roe's flux difference splitting [6]. The primitive-variable extrapolation of the MUSCL approach with a Koren limiter is employed for higher order spatial accuracy [7]. AF-ADI time marching method is adopted to perform time accurate numerical integration [8].

3. BEM

BEM is based on expressing the acoustic pressure at a point within the acoustic medium as an integral over the boundary defining the acoustic domain, which is known as the Helmholtz/Kirchhoff integral equation [9]

$$C(\vec{r})p(\vec{r}) = \int_{S_Y} \left(G(\vec{r},\vec{r}_Y)\frac{\partial p(\vec{r}_Y)}{\partial \hat{n}_Y} - \frac{\partial G(\vec{r},\vec{r}_Y)}{\partial \hat{n}_Y} p(\vec{r}_Y) \right) \mathrm{d}S_Y, \tag{2}$$

where S_Y is the surface of the boundary element model, Y indicates a source point on the boundary element surface, $\vec{r}$ is the position vector for the data recovery point, $\vec{r}_Y$ is the position vector of a source point on the surface of the model, $\hat{n}_Y$ is the unit normal at the location of the source point, $C(\vec{r})$ is the integration constant resulting from the integration of Dirac's function originating from the fundamental solution to the governing differential wave equation, and $G(\vec{r},\vec{r}_Y)$ denotes the Green function as follows:

$$G(\vec{r},\vec{r}_Y) = \frac{1}{4\pi|\vec{r}-\vec{r}_Y|}\mathrm{e}^{-\mathrm{j}|\vec{r}-\vec{r}_Y|}. \tag{3}$$

In order to derive the integral equation for indirect formulation, the standard approach used in indirect boundary element formulations is applied [10,11]. The integral equations for the two acoustic spaces are added together. Within the integral, the terms which include the Green function are factored out and the opposite direction of the unit normal between the two equations is taken into account in generating the new primary variables. The equations for the primary variables and the acoustic pressure at a data recovery point are

$$\delta p(\vec{r}_Y) = p(\vec{r}_{Y_1}) - p(\vec{r}_{Y_2}), \quad \delta\,\mathrm{d}p(\vec{r}_Y) = \frac{\partial p(\vec{r}_{Y_1})}{\partial \hat{n}_{Y_1}} - \frac{\partial p(\vec{r}_{Y_2})}{\partial \hat{n}_{Y_2}}, \tag{4}$$

$$p(\vec{r}) = \int_{S_Y} \left(G(\vec{r},\vec{r}_Y)\delta\,\mathrm{d}p(\vec{r}_Y) - \frac{\partial G(\vec{r},\vec{r}_Y)}{\partial \hat{n}_Y}\delta p(\vec{r}_Y) \right) \mathrm{d}S_Y, \tag{5}$$

where $\delta p(\vec{r}_Y)$ is the difference in pressure between the two sides of the boundary, and $\delta\,\mathrm{d}p(\vec{r}_Y)$ is the difference in the normal gradient of the pressure.

In order to evaluate the primary variables on the surface of the boundary element model, it is necessary to take the boundary conditions into account. In the areas of boundary with pressure boundary condition, $\delta\,\mathrm{d}p$ becomes the unknown variable, while in areas of the boundary with velocity or impedance boundary condition, δp comprises the unknown variable. The pressure boundary condition is applied to represent the noise source

$$\bar{p}(\vec{r}_X) = \int_{S_Y} \left(G(\vec{r}_X,\vec{r}_Y)\delta\,\mathrm{d}p(\vec{r}_Y) - \frac{\partial G(\vec{r}_X,\vec{r}_Y)}{\partial \hat{n}_Y}\delta p(\vec{r}_Y) \right) \mathrm{d}S_Y, \tag{6}$$

where $\vec{r}_X$ is the position vector on the surface of the boundary element model where the acoustic pressure is evaluated. Eq. (6) relates the values of the prescribed pressure, $\bar{p}(\vec{r}_X)$ to the distribution of the primary variables, $(\delta\,\mathrm{d}p(\vec{r}_Y), \delta p(\vec{r}_Y))$ over the surface of the boundary element model. The velocity boundary condition is used to consider the openings, which are expressed as the free edges in the BEM

$$-\mathrm{j}\rho\omega\bar{v}(\vec{r}_X) = \frac{\partial p(\vec{r}_X)}{\partial \hat{n}_X} = \int_{S_Y}\left(\frac{\partial G(\vec{r}_X,\vec{r}_Y)}{\partial \hat{n}_X}\,\delta\,\mathrm{d}p(\vec{r}_Y) - \frac{\partial^2 G(\vec{r}_X,\vec{r}_Y)}{\partial \hat{n}_X \partial \hat{n}_Y}\,\delta p(\vec{r}_Y)\right)\mathrm{d}S_Y. \tag{7}$$

Eq. (7) relates the values of the known surface velocities, $\bar{v}(\vec{r}_X)$ to the distribution of the primary variables, $(\delta\,\mathrm{d}p(\vec{r}_Y), \delta p(\vec{r}_Y))$ over the surface of the boundary element model.

The numerical system of equations for the indirect BEM is derived by a variational principle from the integral equations that originate from the boundary conditions. Unlike the collocation approach that produces non-symmetric matrices, the variational approach results in symmetric system matrices. The variational formulation is based on the principle that the solution to Eq. (8) will also minimize the functional presented in Eq. (9) [12–14]

$$f = \Re(\phi), \tag{8}$$

$$F(\phi) = \int_S \phi\Re(\phi)\,\mathrm{d}S - 2\int_S \phi f\,\mathrm{d}S, \tag{9}$$

where $\Re(\phi)$ is the operator on the unknown function. Here, f is a known function, and $F(\phi)$ is a quadratic functional. The left-hand terms of Eqs. (6) and (7) correspond to f of Eq. (8), and the integrals in Eqs. (6) and (7) correspond to the operator, $\Re(\phi)$ of Eq. (8).

4. Results and discussion

A small-sized centrifugal compressor impeller is used to demonstrate the noise prediction capability. It consists of 12 impeller blades and 12 splitters, and is designed to operate in the counterclockwise rotation at a speed of 70 000 r.p.m. The fundamental BPF values in the inlet and the outlet of the impeller are 14 000 and 28 000 Hz, respectively. Fig. 1 shows the impeller model for performing flowfield analysis and noise prediction.

The impeller design is performed by Samsung Techwin Co., Ltd. using commercial softwares such as COMPAL and DENTON [15]. The flow field of the optimized impeller shows no separation phenomenon in the design point. This justifies the use of an unsteady three-dimensional Euler solver instead of a full three-dimensional Navier–Stokes solver. The simplification results in an affordable computer time while maintaining the useful information on the dynamics of the flow.

As can be seen in Fig. 2, the pressure distribution result obtained using the Euler solver shows pressure fluctuations as well as favorable static pressure increase. The time-dependent pressure data are calculated and are Fourier transformed to examine the effects of the unsteady flow variations in detail. The pressure history in Fig. 3 shows the periodicity due to the rotating

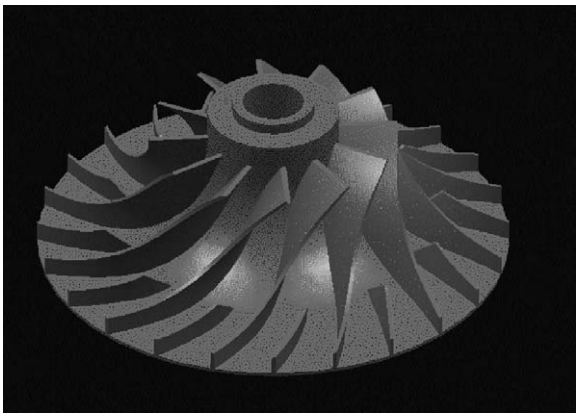

Fig. 1. Impeller model geometry.

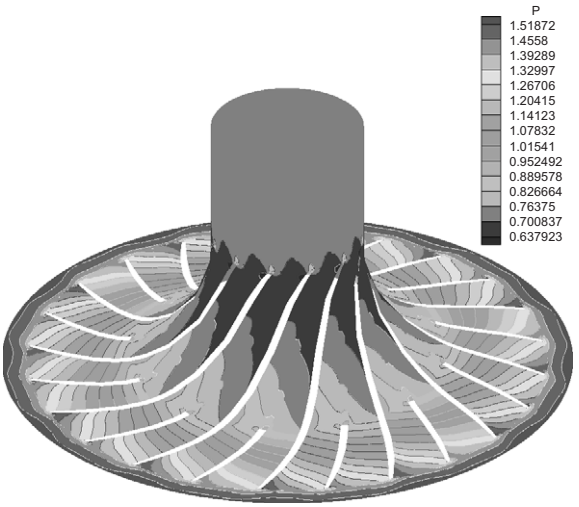

Fig. 2. Static pressure contour by Euler solver.

impeller. The complicated shape in the outlet of the impeller is caused by the mixing flow of the impeller exit and the interaction between the blade and the splitter [16]. The first BPF and its harmonics are dominant in the frequency domain and the sub-harmonic component of 14 000 Hz resulting from the influence of the impeller blade is found in the outlet (Fig. 4).

FW-H equation of the point dipole assumption is used to define the noise source of the centrifugal compressor impeller [17]

$$p(\vec{x},t)=\frac{\cos\theta f}{4\pi}\left\{\frac{\mathrm{i}\omega}{rc}+\frac{1}{r^2}\right\}\mathrm{e}^{\mathrm{i}\omega(t-r/c)}. \tag{10}$$

In Eq. (10) $p(\vec{x},t)$ is the acoustic pressure, $\cos\theta$ is the directivity factor, f is the source strength, ω is the radiated frequency, r is the distance between the source and the observer point, and c is the speed of sound. The near- and farfield components are seen explicitly as $1/r^2$ and $1/r$ terms,

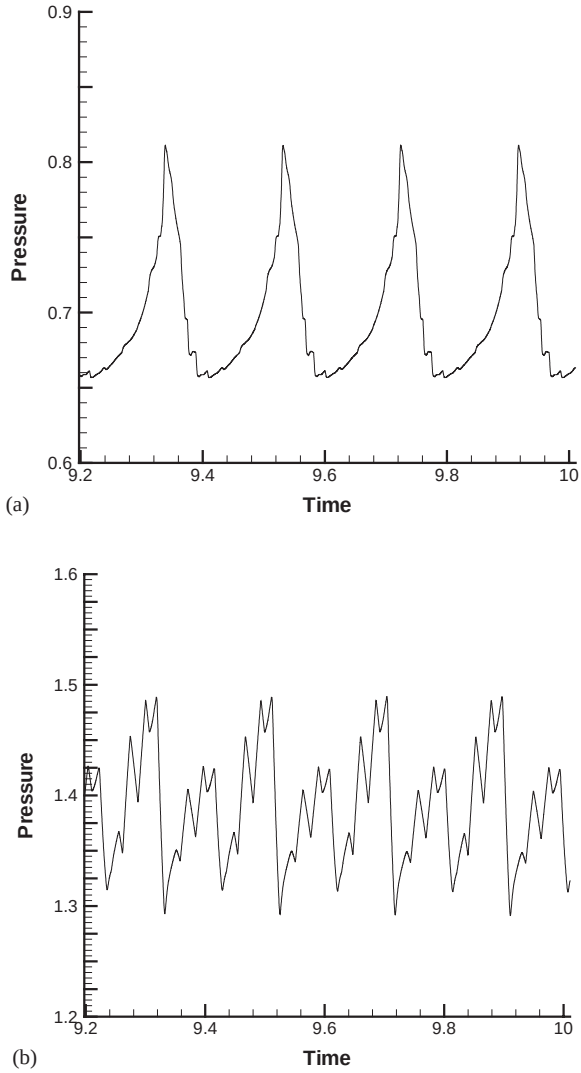

Fig. 3. Pressure fluctuations in the time domain: (a) Impeller inlet part and (b) impeller outlet part.

respectively. The acoustic pressure boundary conditions, which are the input data of BEM analysis are obtained from the combination of FW-H formulation and computed pressure spectrum.

The noise measurements are performed to comprehend the aerodynamic noise features of the centrifugal compressor and to present the research direction for developing the noise prediction technique. In Fig. 5a, the noise spectrum is measured at a distance of 1.5 m from the centrifugal compressor center. The position in front of the inlet duct end is chosen to minimize the influence of other noise components on the centrifugal compressor system.

From the measured noise spectrum, the discrete peak of 14 000 Hz (indicated by the arrow, → in Fig. 5b) and the sub-harmonic component of 7000 Hz (indicated by the arrow, → in Fig. 5b)

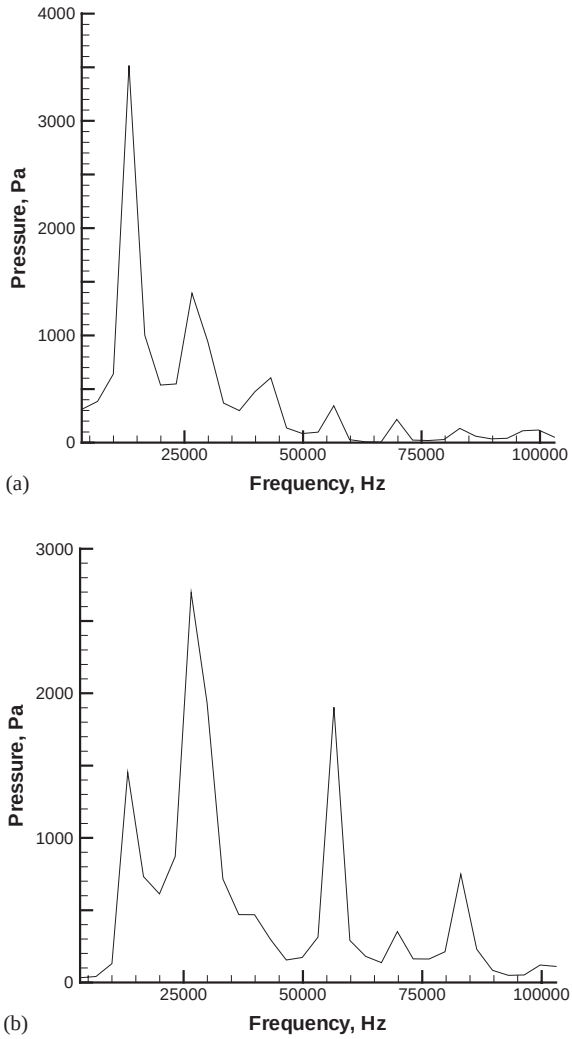

Fig. 4. FFT distributions in the frequency domain: (a) Impeller inlet part and (b) impeller outlet part.

are found. The low- and medium-frequency noise caused by other components of the centrifugal compressor and broadband noise are not considered here because this work is focused on the aerodynamic BPF noise of the impeller.

The noise level at the dominant frequency of 14 000 Hz is calculated to validate the prediction method incorporating Euler equations, noise source definition method, and BEM solver. Because of the computation time, the assumptions that the inlet and the volute outlet are open at the fixed positions have been incorporated in the calculation, which is not the actual case. The BEM mesh consists of inlet duct, diffuser, and volute as shown in Fig. 6a. From the directivity pattern of Fig. 6b, it is observed that the impeller noise is propagated through the duct and is diffracted in the free field. The noise distribution from the volute outlet seems to be random because of the complex geometries including the diffuser and the volute.

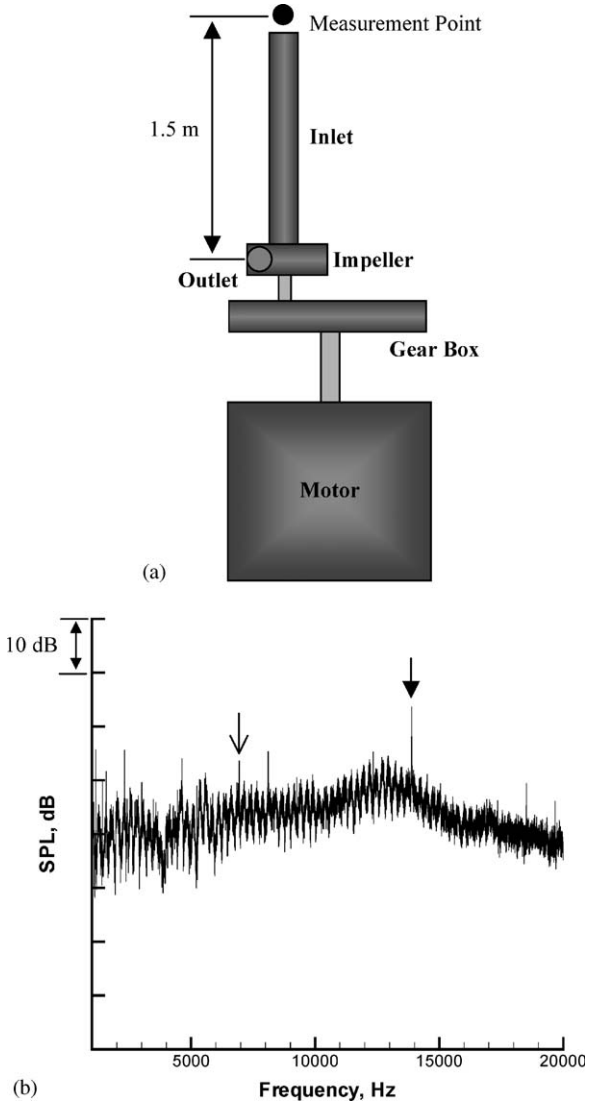

Fig. 5. (a) Experimental set-up for noise measurement and (b) measured noise spectrum.

For the validation of the numerical method, the SPL values are computed at the fundamental BPF and the sub-harmonic frequencies. As can be seen in Fig. 7, the numerical results at the discrete frequencies are predicted with sufficient accuracy.

5. Concluding remarks

In the present study, numerical prediction method of centrifugal compressor noise is introduced. Euler solver is used to analyze the flow field around the impeller and the unsteady

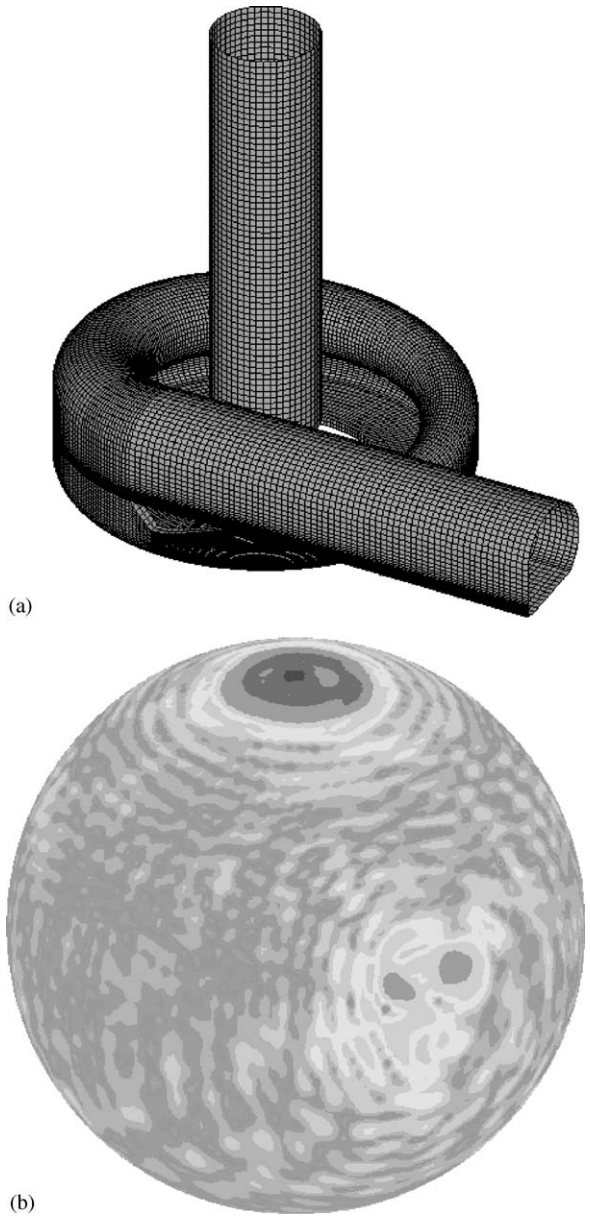

Fig. 6. (a) BEM mesh of centrifugal compressor and (b) directivity pattern of noise propagation.

pressure fluctuations from the inlet and the outlet of the impeller. FW-H formulation is applied to estimate the noise source and indirect variational BEM is employed to take the noise propagation into account. The spectrum analysis of the measured noise shows that the aerodynamic BPF noise of the impeller is dominant. The calculation results are compared with the experimental data. The comparison of the measured and calculated result shows good agreement.

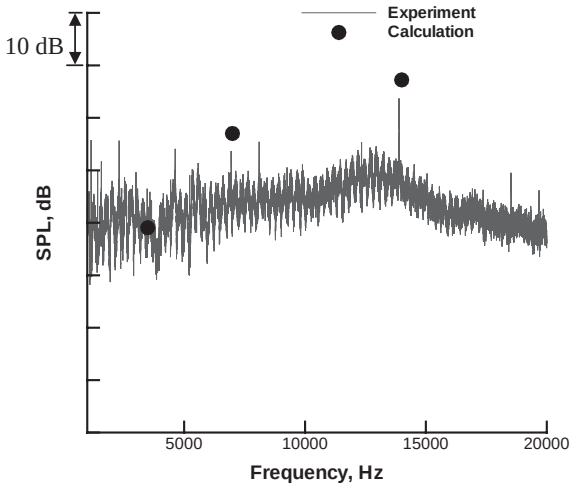

Fig. 7. Comparison of computation results and experimental data.

Acknowledgements

The authors acknowledge the support for this research work by Samsung Techwin Co., Ltd.

References

[1] A. Stirnemann, H. Zogg, F. Stocker, Prediction of turbo compressor noise, Inter-Noise, Florida, USA, 1999.
[2] W. Jeon, J. Lee, A study on the noise reduction method of a centrifugal compressor, Inter-Noise, Hague, Netherlands, 2001.
[3] S. Chu, R. Dong, J. Katz, Unsteady flow, pressure fluctuation and noise associated with the blade tongue interaction in a centrifugal pump, ASME Symposium Flow Noise Modelling, Measurement and Control, ASME WAM, New Orleans, 1993.
[4] R. Dong, S. Chu, J. Katz, Effect of modification to tongue and impeller geometry on unsteady flow, pressure fluctuations and noise in a centrifugal pump, Journal of Turbomachinery 119 (1997) 506–515.
[5] H. Uchida, M. Inayoshi, K. Sugiyama, Effect of a circumferential static pressure distortion on small-sized centrifugal compressor performance, Presented at the International Gas Turbine Congress held in Tokyo, Japan, 1987.
[6] P.L. Roe, Approximate Riemann, solvers parameter vectors, and difference schemes, Journal of Computational Physics 43 (1981) 357–372.
[7] P.K. Sweby, High resolution TVD schemes using flux limiters, Lectures in Applied Mathematics 22 (1985) 289–309.
[8] T.H. Pulliam, D.S. Chaussee, A diagonal form of an implicit approximate-factorization algorithm, Journal of Computational Physics 39 (1981) 347–365.
[9] R.D. Cickowski, C.A. Brebbia, Boundary Element Methods in Acoustics, Elsevier Applied Science, New York, 1991.
[10] P.K. Banerjee, The Boundary Element Methods in Engineering, McGraw-Hill, New York, 1994.
[11] T.W. Wu, Boundary Element Acoustics, WIT Press, Southampton, 2000.
[12] M.A. Hamdi, J.M. Ville, Sound radiation from ducts: theory and experiment, Journal of Sound and Vibration 107 (1986) 231–242.
[13] S.G. Mikhlin, Variational Methods in Mathematical Physics, MacMillan, New York, 1964.

[14] N. Vlahopoulos, S.T. Raveendra, Formulation, implementation and validation of multiple connection and free edge constraints in an indirect boundary element formulation, Journal of Sound and Vibration 210 (1998) 137–152.
[15] J.D. Denton, An improved time-marching method for turbomachinery flow calculation, Journal of Turbomachinery 105 (1983) 514–524.
[16] D. Japikse, Centrifugal Compressor Design and Performance, Concepts ETI, Inc., USA, 1996.
[17] A.P. Dowling, J.E. Ffowcs Williams, Sound and Sources of Sound, Wiley, New York, 1983.